Article

High Performance Polymers

High Performance Polymers
1–15

DOI: 10.1177/0954008317734034
journals.sagepub.com/home/hip

Novel fluorinated hyperbranched polyimides with excellent thermal stability, UV-shielding property, organosolubility, and low dielectric constants

Qing Li, Shulai Zhang, Guangfu Liao, Changfeng Yi and Zushun Xu

Abstract

A novel fluorinated aromatic triamine, named 1,3,5-tris (4-(2-trifluoromethyl-4-aminophenoxy)phenyl) benzene (TTFA-POPB), with several $-CF_3$ groups, prolonged chain segments, and ether bonds was first successfully synthesized via a three-step reaction. Then a series of fluorinated hyperbranched polyimides (FHBPIs) with terminal amino or anhydride groups were prepared by condensation polymerization, which were derived from three commercial dianhydrides and the obtained triamine. The prepared FHBPIs showed excellent optical properties with the transmittance reaching 94.5% at 800 nm, favorable ultraviolet (UV)-shielding property with only 27% photodegradation of methylene blue solution after intense UV irradiation for 50 min, good thermal stability with glass transition temperature between 225°C and 264°C, and 10% weight loss temperature of 520–555°C and 509–541°C, respectively, in nitrogen and air atmosphere. They also exhibited relatively good mechanical properties with tensile strength, tensile modulus, and elongation at break values of 64.2–84.2 MPa, 1.2–1.5 GPa, and 6–10%, respectively. Moreover, the introduction of $-CF_3$ and hyperbranched architecture reduced the dielectric constants of the FHBPIs to 2.69–2.92 and increased the surface contact angles to more than 98°. Thus, the FHBPIs are promising dielectric or UV-shielding materials.

Keywords

Fluorinated hyperbranched polyimides, monomer synthesis, thermal stability, UV shielding, low dielectric constants

Introduction

Over the past years, hyperbranched polymers (HBPs) have attracted extensive attention in the fields of chemistry, biology, and biomedicine because the HBPs do not have complete branching structure, whereas they also have physical properties similar to dendrimers, and for most cases, they can be used to replace dendrimers.[1–4] Additionally, HBPs can be prepared by one-step polymerization with multifunctional monomers, which is rather more convenient than the synthesis procedure of dendrimers. Thus, many kinds of HBPs have come forth in recent years, including polyimide (PI),[5] poly (ether ketone), polyester,[6] and polyurethane.[7] Apart from the research on the structure of HBPs, more and more studies are focused on their new applications, such as optical and electronic materials,[8,9] polymer electrolytes,[10] nanotechnology,[11] and other high-tech areas.[12–14]

PIs, as a kind of important high-performance polymer material, have many prominent properties such as excellent thermal stability, good mechanical properties, considerable optical properties, electrical properties, and low coefficient of thermal expansion.[15–19] As a result, they are always applied in photoresist, adhesive, and electronic instrument,

Hubei Collaborative Innovation Center for Advanced Organic Chemical Materials, Ministry of Education Key Laboratory for the Green Preparation and Application of Functional Materials, Hubei University, Wuhan, Hubei, China

Corresponding author:
Zushun Xu, Hubei Collaborative Innovation Center for Advanced Organic Chemical Materials, Ministry of Education Key Laboratory for the Green Preparation and Application of Functional Materials, Hubei University, Wuhan, Hubei 430062, China.
Email: zushunxu@hubu.edu.cn

or used as matrix for composites.[20–24] However, their further applications are always limited by their poor processability because of their poor solubility in common organic solvents or their high melting point and high glass transition temperature (T_g).[25] It has been shown that $–CF_3$ substituents can be of considerable interest to material chemists. Steric congestion and strong electronegativity imparted by the $–CF_3$ group actually result in less efficient chain packing, so the solubilities of PIs can be considerably improved through the introduction of $–CF_3$ groups.[26–28] The $–CF_3$ groups could also increase free volume, which is occupied by air. This in turn results in a decrease in dielectric constants of PIs.[29] Moreover, with $–CF_3$ groups inducing separation of the chain backbones, the formation of charge transfer complex (CTC) is largely hindered, and thus, the color intensity of PI is considerably reduced, making the PI more suitable for some advanced applications.[30] In addition, fluorinated hyperbranched polyimides (FHBPIs) have very large cutoff wavelengths (more than 400 nm), and their transmittances in the visible region are very high. Hence, they are also promising ultraviolet (UV)-shielding materials.

Generally speaking, hyperbranched polyimides (HBPIs) are always easily synthesized by condensation polymerization of AB_2 or $A_2 + B_3$ monomers in which A and B refer to anhydride and amine groups, respectively. However, due to the high reactivity between anhydride and amine groups, AB_2 monomers are very difficult to prepare.[31–33] The preparation of HBPIs by $A_2 + B_3$ is a more facile method. Thus, new triamine monomers need to be designed and synthesized, especially for the triamine monomers that contain $–CF_3$ groups, ether bonds, and prolonged chain segments. In this article, a novel fluorinated symmetrical triamine monomer, 1,3,5-tris (4-(2-trifluoromethyl-4-aminophenoxy)phenyl) benzene (TTFAPOPB), with prolonged chain segments, ether bonds, and $–CF_3$ groups was successfully synthesized. Then a series of FHBPIs were prepared by $A_2 + B_3$ polycondensation using various commercial aromatic dianhydrides and the prepared TTFAPOPB. Compared with 1,3,5-(2-tri-fluoromethyl-4-aminophenoxy) benzene (TFAPOB), which was synthesized by Hong et al.,[34] the TTFAPOPB had several prolonged chain segments and ether bonds, which endowed the resulting PIs with flexible chain structure, increased free volume, and reduced crystallinity. Hence, our prepared PIs showed improved solubilities. Moreover, compared with the triamine 1,3,5-tris[4-(4-a-midophenoxy)phenyl] benzene (TAPOPB), which referred to our previous work,[35] the FHBPIs synthesized from TTFAPOPB showed better thermal stability, electrical, and optical properties. In addition, the FHBPIs derived from TTFPOPB exhibited favorable hydrophobicity, low dielectric constants, and high transparency. At the same time, we studied the UV-shielding performance of FHBPIs. Therefore, in the hydrophobic, optical, and electrical fields, the obtained FHBPIs would have a great application prospect.

Experimental

Materials

4-Hydroxyacetophenone (99%), palladium on activated carbon (Pd/C; 5%), hydrazine monohydrate (80 vol%), and 2-chloro-5-nitrobenzotrifluoride (GC, >99.5%) were purchased from Sigma (St. Louis, MO); 3,3′,4,4′-benzophenonetetracarboxylic dianhydride (BTDA) and 2,2′-bis[4-(3,4-dicarboxyphenoxy)phenyl]propane dianhydride (BPADA, 98%) were purchased from Shanghai Research Institute of Synthetic Resins (Shanghai, China); 4,4-(hexafluoroisopropylidene) diphthalic anhydride (6FDA) were obtained from J & K Scientific Ltd (Beijing, China). These aromatic tetracarboxylic compounds were recrystallized from acetic anhydride and dried in oven at 100°C for 12 h before use. *N*-methyl-2-pyrrolidone (NMP) and m-xylene were distilled from calcium hydride under reduced pressure. Anhydrous potassium carbonate (K_2CO_3; analytical) was dried in vacuum at 120°C for 12 h before use.

Measurements

The Fourier-transform infrared (FTIR) spectra were recorded on a Perkin–Elmer spectrometer (Spectrum One, Waltham, MA), and powder samples were taken into performing with kiln-dried KBr powder. Proton nuclear magnetic resonance (^{1}H-NMR) was performed on a Varian INOVA-600 spectrometer (Salt Lake City, Utah, USA) at 600 MHz with tetramethylsilane as a reference and hexadeuterated dimethyl sulfoxide (DMSO-d6) as solvent. The wide-angle X-ray diffraction (WAXD) was performed at 40 kV and 40 mA using a XPERT PRO apparatus with a Cu-Kα ($\lambda = 0.154$ m) source at 293 K, and the scanning rate was 10°/min over a range at $2\theta = 5–80°$. The solubility was measured by dissolving (10 mg) polymers into (1 mL) several different organic solvents at room temperature or on heating, and after 24 h, dissolving properties were checked and recorded. Differential scanning calorimetry (DSC) was operated with a heat rate of 20°C/min from 100°C to 320°C under nitrogen atmosphere on a Perkin–Elmer DSC-7 system. The dynamical mechanical thermal analysis (DMTA) was obtained on a Du Pont TA Instruments DMA Q800 (New Castle, Pennsylvania, USA) in a tension mode at a frequency of 1 Hz and a heating rate of 5°C/min from 100°C to 400°C in air. Thermogravimetric analysis (TGA) was carried out uisng a Perkin–Elmer TGA-7 thermal gravimetric analyzer, from 30°C to 800°C with a heating rate of 20°C/min under nitrogen and air atmosphere. The mechanical properties were performed on a CMT4104 electromechanical universal testing machine (Shenzhen SANS Testing Machine Co., Ltd., Shenzhen, China) at room temperature, with a load of 100 N and pulling rate of 5 mm/min. The samples were made into 5 mm wide and 50 mm long. Ultraviolet–visible spectroscopy was performed in the transmittance mode on

a Shimadzu UV-3600 spectrometer. The thickness of all films were maintained at 0.16 mm. The dielectric constant (ε) was obtained at 1 MHz using an independent gain phase analyzer (HP4194A), and the formula is $\varepsilon = Cd/A\varepsilon_0$, where C is the observed capacitance, d is the film thickness, A is the area, and ε_0 is the free permittivity. Harrick Plasma PDC-32A (New York, USA), the plasma cleaner, was used to treat the HBPIs by indium tin oxide (ITO) plates. The thickness of each film is 160 $\pm$ 10 μm. Surface contact angle (SCA) test was conducted on JC2000 D instrument (Shanghai, China). Water absorption (WA) was determined by immersing dried film samples into deionized water for 24 h at 25°C, then weighing them after fast drying surface moistures. The values were calculated using the equation from our previous work.[36]

UV-shielding measurement of FHBPI films was designed. The thickness of each film was 160 $\pm$ 10 μm. In order to evaluate the UV-shielding performance of films under strong UV irradiation, the degradation behavior of methylene blue (MB) solution in the presence of photocatalyst (nano-TiO_2) under high-pressure mercury lamp (400 W) was applied. Before UV irradiation, 10 mg of TiO_2 nanoparticles was added to a vial, which was covered by tinfoil and filled with 20 mL of MB solution. Then the suspension was constantly stirred in the dark for 40 min to reach adsorption–desorption equilibrium. The distance between the lamp and the mouth of the vial was about 15 cm. The photocatalytic degradation of MB solution was carried out under constant stirring. First, we set a blank control experiment in which the MB solution was directly exposed to UV light without the shielding of any films. Then the FHBPIs films were used to cover the mouth of the vial. At a given time (t), 6 mL of the suspension was collected and centrifuged to remove the photocatalyst. The absorbance of MB solution at 665 nm was measured by a Shimadzu UV-3600 spectrometer (Perkin-Elmer, Waltham, Massachusetts, USA). The UV-shielding performance was calculated as $I = A_t/A_0 \times 100\%$, where A_0 is the initial absorbance of MB solution after adsorption–desorption equilibrium and A_t is the absorbance of the remaining MB solution shielded with film under UV radiation.

Synthesis of fluoro-triamine monomer

4-(2-trifluoromethyl-5-nitrophenoxy)-acetophenone (TFNPAP)

In a 250-mL three-necked round-bottomed flask equipped with mechanical stirrer, 4-hydroxyacetophenone (13.62 g) and K_2CO_3 (17.28 g) were dissolved in 80-mL *N*, *N*-dimethylacetamide (DMAC), and the mixture was heated at 120°C with reflux condenser and stirred for 3 h under nitrogen. To the mixed solution, 2-Chloro-5-nitrobenzotrifluoride (22.56 g) was added when the temperature cooled down to 60°C naturally, followed by heating at 120°C with sequentially stirring for 12 h. After the temperature cooled down to 60°C again, the mixture was poured into 100-mL (10 vol%) ethanol aqueous solution. The yield of yellow precipitate was collected by filtration and washed several times with deionized water. Eventually, the product was recrystallized in ethanol and dried in vacuum at 80°C to obtain 29.480-g TFNPAP.

Yield: 29.48 g (75.27 wt%). FTIR (KBr, cm^{-1}): 3090, 2864 (C–H); 1680 (C=O); 1421 (–CH_3); 1350 (–NO_2); 1050 (C–F); 840 (C–N); ^{1}H-NMR (600 MHz, DMSO-d_6, δ): 2.58 (s, 3H); 7.24–7.26 (d, 2H); 7.31–7.32 (d, 1H); 8.07 (d, 2H); 8.47–8.49 (d, 1H); 8.53 (s, 1H). Theoretical calculation for $C_{15}H_{10}O_4N_1F_3$ (325.24): C, 55.34%; H, 3.08%; N, 4.31%. Elemental analysis test: C, 55.81%; H, 2.92%; and N, 4.40%.

1,3,5-Tris(4-(2-trifluoromethyl-4-nitrophenoxy)phenyl)benzene (TTFNPOPB)

In a 250-mL three-necked round-bottomed flask, the prepared TFNPAP (19.53 g) and 48-mL absolute ethyl alcohol were added, and then a dropping funnel was linked with a drying pipe, which was filled with calcium chloride and connected to an absorption apparatus. Afterward, silicon tetrachloride (TCS) (17 mL) was added to the dropping funnel with an injection. Along with vigorous magnetic stirring, TCS was added dropwise into the flask. After the drop was finished, the mixture was continuously stirred for another 14 h at room temperature to yield a deep red solution with some precipitation. Subsequently, 100-mL deionized water was added to the mixture solution for several times and then the mixture solution was stirred for an additional 0.5 h. Then the sodium hydroxide aqueous with a mass fraction of 10% was added until the red solution turned orange. The product was collected by filtration and washed with deionized water and refluxed in (95 vol%) ethanol aqueous solution for 0.5 h at 80°C. After the solution cooled down to room temperature, the light yellow powder was obtained by filtration. Finally, the product was recrystallized in ethanol and CH_2Cl_2 mixing solution, and 10.87 g of acicular crystals was obtained.

Yield: 10.87 g (58.99 wt%). FTIR (KBr, cm^{-1}): 3090, 2864 (C–H); 1350 (–NO_2); 1050 (C–F); 840 (C–N); ^{1}H-NMR (600 MHz, DMSO-d6, δ): 7.19–7.21 (d, 3H); 7.29–7.36 (d, 6H); 7.98 (s, 3H), 8.06–8.07 (d, 6H); 8.49–8.51 (d, 3H); 8.53 (s, 3H). Theoretical calculation for $C_{45}H_{24}O_9N_3F_9$ (921.672): C, 58.62%; H, 2.62%; N, 4.56%. Elemental analysis test: C, 58.15%; H, 2.65%; N, 4.66%.

TTFAPOPB

In a 250-mL three-necked round-bottomed flask, the obtained TTFNPOPB (9.49 g) and 0.6 g of palladium on activated carbon (Pd/C, 5%) were completely dispersed in 100-mL absolute ethyl alcohol and then heated to reflux

temperature at 80°C accompanied by vigorous stirring under nitrogen atmosphere. Twenty milliliters of hydrazine monohydrate was added dropwise into the flask for 2 h. After stirring and refluxing for 12 h, the solution was filtrated while hot. Finally, the obtained flocculent filtrate was collected by pouring the filtrate into an 800-mL deionized water. Through filtration, washing, and drying, approximately 7.84 g of TTFAPOPB was obtained.

Yield: 7.84 g (94.29 wt%). FTIR (KBr, cm^{-1}): 3316, 3207 (Ar–NH_2); 3090, 2864 (C–H); 1050 (C–F); 840 (C–N); ^{1}H-NMR (600 MHz, DMSO-d6, δ): 5.48 (s, 6H); 6.79–6.80 (d, 6H); 6.89 (s, 3H); 6.90–6.92 (d, 6H); 7.70 (s, 3H); 7.74–7.75 (d, 6H). Theoretical calculation for $C_{45}H_{30}O_3N_3F_9$ (831.72): C, 64.93%, H, 3.61%, N, 5.05%. Elemental analysis test: C, 64.13%; H, 3.52%; N, 5.87%.

Preparation of FHBPIs

Preparation of amino-terminated FHBPIs (AM-FHBPIs)

AM-FHBPIs were synthesized by a typical two-step method. First, in a three-necked, round-bottomed flask, 1.0 mmol of TTFAPOPB was dissolved in a 10-mL NMP with magnetic stirring and nitrogen flow. Then 1.0-mmol dianhydride was also dissolved in 10-mL NMP. Subsequently, the anhydride solution was added dropwise into the flask for 4 h at 40°C. After the drop was completed, the mixture solution was stirred for additional 24 h, and the hyperbranched polyamine acid (HBPAA) solution was generated. Eventually, the obtained HBPAA solution was casted on glass plates at 100°C for 12 h to evaporate the solvent, and then thermal imidization was performed by programmed heating (150, 200, 250, and 300°C for each 1 h, respectively) in air. The obtained AM-FHBPI membranes were peeled off from the glass plates. The chemical imidization was conducted by adding 5 drops of isoquinoline and (15 mL) x-xylene into the HBPAA solution and stirring it continuously at 120°C for 3 h and at 180°C for 24 h, respectively. After cooling down to room temperature, the solution was poured into (300 mL) EtOH to yield a powder precipitate. By filtration and washing, the obtained AM-FHBPIs were dried in a vacuum oven at 80°C for 24 h.

Preparation of anhydride-terminated FHBPIs (AD-FHBPIs)

The AD-FHBPIs were prepared by following the same steps used for preparing AM-FHBPIs, except for the different molar ratios and addition of an order of monomers. In a 100-mL three-necked, round-bottomed flask, 1 mmol of dianhydride was dissolved in 10-mL NMP under nitrogen atmosphere at 40°C. TTFPOPB (0.5 mmol) was dissolved in 10-mL NMP and then the obtained solution was added dropwise into the flask for 4 h. The anhydride-terminated HBPAA solution was obtained after additional stirring for 24 h. Finally, the HBPAA solution was poured on a glass plate, heating to 100°C for 12 h to evaporate the solvent. The obtained HBPAA films were converted into HBPI films through programmed heating (the same to the AM-FHBPIs). The chemical imidization was performed with the following steps: First, 1.2 mL anhydride and 0.6 mL pyridine were added into the HBPAA solution; second, the mixture was stirred at 60°C for 6 h, 80°C for 2 h, and 100°C for 2 h, respectively; eventually, the mixture solution was poured into 300 mL EtOH to yield a powder precipitate. By filtrating and washing, the obtained FHBPIs were dried in a vacuum oven at 80°C for 24 h.

Results and discussion

Synthesis of fluoro-triamine monomer

It takes three steps to synthesize the novel fluoro-triamine; the specific procedure is shown in Figure 1. In the first step (a), under the effect of anhydrous potassium carbonate, nucleophilic substitution reactions were accomplished between 4-hydroxyacetophenone and 2-chloro-5-nitrobenzotrifluoride, generating the intermediated product TFNPAP. In the second step (b), the fluoro-trinitro compound, TTFNPOPB, was synthesized by a condensation reaction of three molecules of TFNPAP with the STC/EtOH acting as catalyst. The STC/EtOH was an excellent and effective catalyst in the synthesis of polystyrene ring macromolecules accompanied by a mild synthesis condition and high yield. In the last step (c), with the hydrazine hydrate and Pd/C acting as reductant and catalyst, respectively, the obtained TTFNPOPB was reduced to TTFAPOPB.

FTIR was used to characterize the structure of the three products, as shown in Figure 2. The characteristic absorption band at 1350 cm^{-1}, which can be only seen in curves a and b, is the characteristic absorption peak of –NO_2. However, in curve c, the –NO_2 absorption peak was not found, but the characteristic vibration peaks of the –NH_2 at 3316 and 3207 cm^{-1} emerged, which proved that the nitro groups of TTFNPOPB were absolutely reduced into amino groups. The absorption peaks at 1680 and 1421 cm^{-1}, which can be only observed in curve a, were associated with the vibration absorption peaks of carbonyl C=O and methyl –CH_3; the C–F and C–N absorption bands could be observed in curves a, b, and c at 1050 and 840 cm^{-1}.

The ^{1}H NMR spectrum of intermediated product TFNPAP is shown in Figure 3a. It can be clearly seen that there is no distinct miscellaneous peaks in the spectrum, and each peak has a very good attribution.

Figure 3b shows the ^{1}H-NMR spectrum of TTFNPOPB. The insert is the enlarged image of the corresponding location. It can be seen that all peaks in the spectrum also have good attributions, and no miscellaneous peaks appeared.

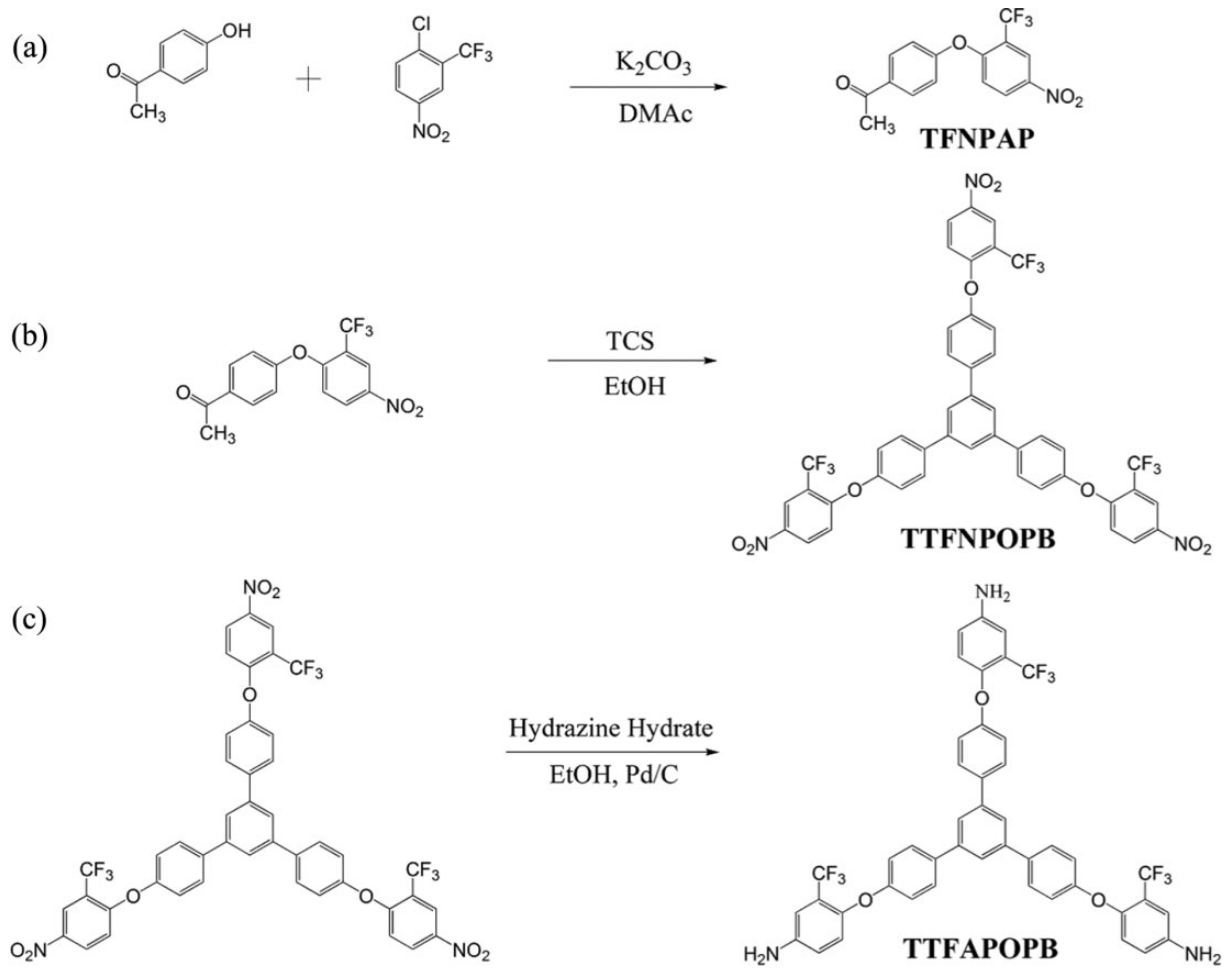

Figure 1. Synthetic process of the novel fluoro-triamine monomer TTFAPOPB. TTFAPOPB: 1,3,5-tris (4-(2-trifluoromethyl-4-aminophenoxy)phenyl) benzene.

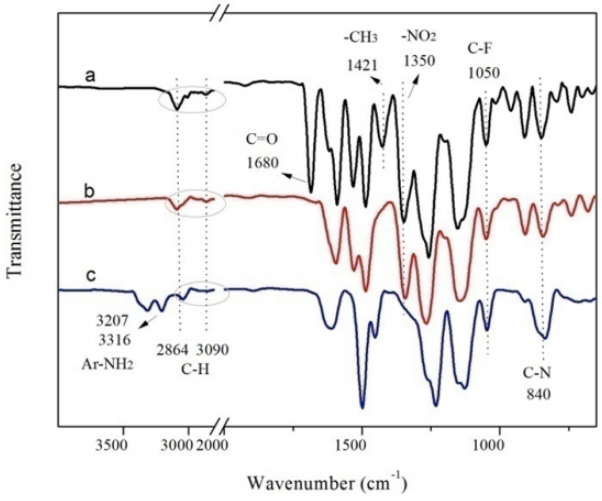

Figure 2. FTIR curves of (a) TFNPAP, (b) TTFNPOPB, (c) TTFAPOPB. FTIR: Fourier-transform infrared; TFNPAP: 4-(2-trifluoromethyl-5-nitrophenoxy)-acetophenone; TTFNPOPB: 1,3,5-tris (4-(2-trifluoromethyl-4-nitrophenoxy)phenyl)benzene; TTFAPOPB: 1,3,5-tris (4-(2-trifluoromethyl-4-aminophenoxy)phenyl) benzene.

The ^{1}H-NMR spectrum of the final product, TTFAPOPB, is shown in Figure 3. Obviously, the new single peak at 5.48 ppm can be seen clearly, which is attributed to the signal peak of H proton in amino, and in the enlarged image of the spectrum, all peaks have corresponding attributions. It is indicated that the TTFNPOPB was completely reduced to TTFAPOPB. Additionally, elemental analysis was used to demonstrate the components of the TFNPAP, TTFNPOPB, and TTFAPOPB monomers. The test results and theoretical values are shown in the experimental section. The test values were in accordance with the theoretical values; it indicated that the obtained TFNPAP, TTFNPOPB, and TTFAPOPB were pure enough for later use.

Preparation of FHBPIs

FHBPIs were prepared by a typical two-step method; the specific procedures are shown in Figure 4. First, three commercially available aromatic dianhydrides (BPADA, BTDA, 6FDA) were used as the A_2-type monomer to react

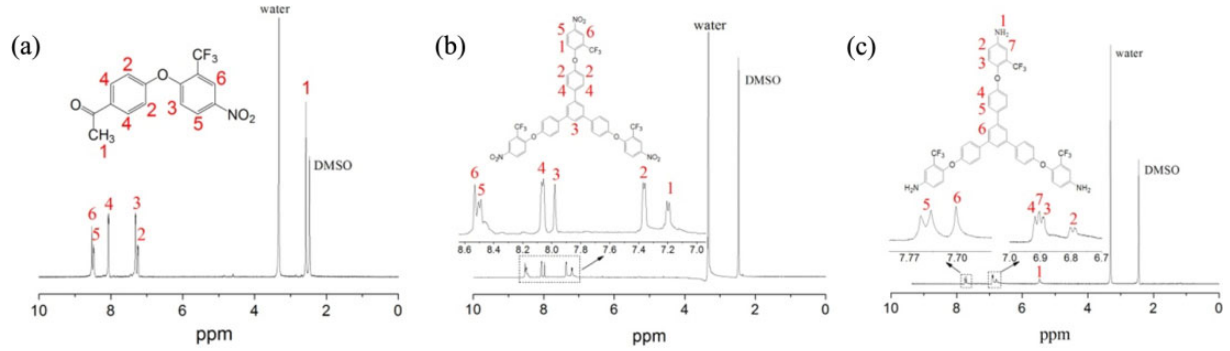

Figure 3. The ^{1}H-NMR spectra of TFNPAP (a), TTFNPOPB (b), TTFAPOPB (c). TFNPAP: 4-(2-trifluoromethyl-5-nitrophenoxy)-acetophenone; TTFNPOPB: 1,3,5-tris(4-(2-trifluoromethyl-4-nitrophenoxy)phenyl)benzene; TTFAPOPB: 1,3,5-tris (4-(2-trifluoro-methyl-4-aminophenoxy)phenyl) benzene; ^{1}H-NMR: proton nuclear magnetic resonance.

with A_3-type monomer TTFAPOPB. The HBPAA solution with different terminal groups was prepared by changing the sequence of adding monomers and molar ratio. Second, by thermal or chemical imidization, the HBPAA was dehydrated to form imide ring and converted to FHBPIs, according to the previous report.[20] The partial chemical structure of the FHBPIs is displayed in Figure 5.

Structural and morphological characterization of FHBPIs

The structure and morphology of FHBPIs were evaluated by FTIR and X-ray powder diffraction (XRD; Figure 6). Figure 6a shows the FTIR spectra of the resulting FBHPIs. In all of the curves, the absorption bands at 1789, 1721, and 737 cm^{-1} appeared, which can be attributed to the two characteristic absorptions of the carbonyl in imide ring. The absorption band around 1055 cm^{-1} was assigned to C–F stretching vibrations, and the C–N stretching vibration band in imide ring was detected at 1386 cm^{-1}. In addition, as seen in curves a, b, and c, the absorption peak at 1853 cm^{-1} is the characteristic one of the terminal anhydride groups' (C–O–C) stretching vibration. In curves d, e, and f, the weak absorption peak at 3501 cm^{-1} was attributed to the characteristic absorption of terminal amine groups. Moreover, the bands at about 2924 and 2857 cm^{-1} in curves a and d are assigned to the $–CH_2$ stretching vibrations derived from BPADA monomer.

The wide-angle X-ray diffractometer was used to detect the morphological information of the FHBPIs, as shown in Figure 6b. Because the steric congestion imparted by the $–CF_3$ group actually disrupts the chain packing, and the introduction of the ether bonds increases the flexibility of the polymer chains, there is no obvious crystallization peak in all of the curves except a blunt diffraction peak. This implies that the obtained FHBPIs have very low degrees of crystallinity, thus leading to excellent solubilities.

Solubilities of FHBPIs

Table 1 exhibits the solubilities of the resulting FHBPIs in relevant solvents. All of the FHBPIs display excellent solubilities in common polar aprotic solvents, such as NMP, *N*, *N*-dimethyformamide (DMF), DMAC, and DMSO. However, in pyridine, m-cresol, tetrahydrofuran (THF), CH_2Cl_2, and $CHCl_3$, the solubilities of the FHBPIs varied with the different dianhydride monomers. AM-BPADA and AD-BPADA possess the best solubilities of all the FHBPIs, which is attributed to the existence of ether bonds in BPADA. AM-BTDA and AD-BTDA showed the worst solubility, which was due to the rigid ketonic linkages in BTDA. The solubilities of the FHBPIs derived from 6FDA were in the middle of them. In addition, compared with the HBPIs derived from 2,4,6-tris[4-(4-aminophenoxy)phenyl]pyridine (TAPPP), a triamine monomer prepared by Chen,[37] the solubility of the FHBPIs derived from TTFAPOPB has shown a great improvement. This is mainly attributed to the bulk volume of the $–CF_3$, the prolonged segments, and ether bonds from TTFPOPB.

Thermal properties of FHBPIs

TGA, DMTA, and DSC were used to investigate the thermal performance of the obtained FHBPIs. The results are summarized in Table 2. In theory, the T_g is the ultimate-use temperature of polymer material. DSC was used to determine the T_g values of the FHBPIs, and the resulting curves are shown in Figure 7a. Results showed that the T_g values were mainly affected by the chemical structure of the aromatic dianhydride. Because of the existence of the rigid BTDA moieties in the polymer backbone, AD-BTDA and AM-BTDA showed the highest T_g at 238 and 264°C, respectively; on the contrary, the FHBPIs derived from BPADA acquired the lowest T_g at 226 and 235°C, respectively, for AD-BPADA and AM-BPADA. This was because BPADA possessed relatively vast flexible segments and ether bonds; moreover, the T_g values of AM-FHBPIs were significantly higher than the corresponding

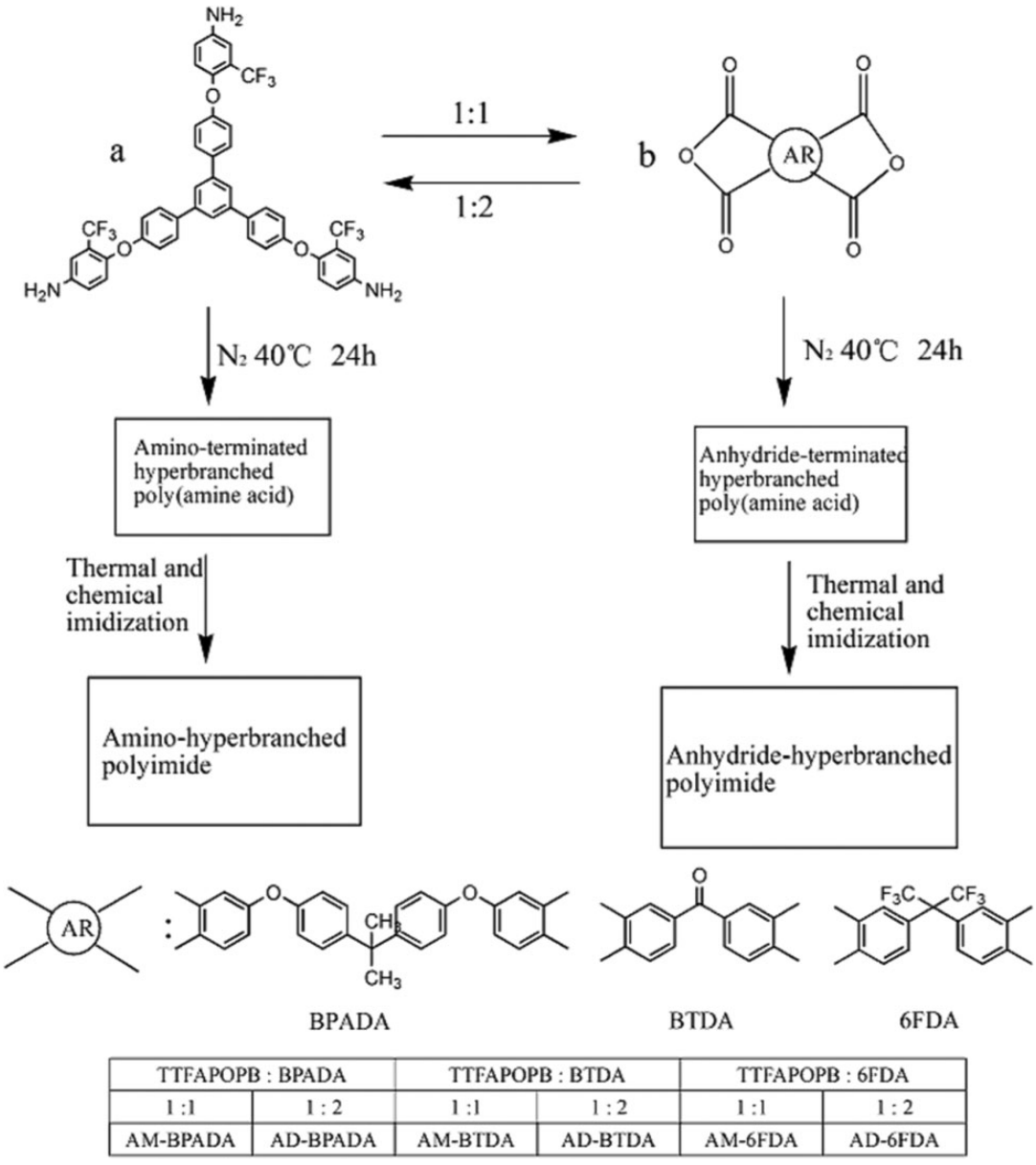

TTFAPOPB : BPADA		TTFAPOPB : BTDA		TTFAPOPB : 6FDA	
1 :1	1 : 2	1 :1	1 : 2	1 :1	1 : 2
AM-BPADA	AD-BPADA	AM-BTDA	AD-BTDA	AM-6FDA	AD-6FDA

Figure 4. Synthetic process of the novel FHBPIs. FHBPIs: fluorinated hyperbranched polyimides.

AD-FHBPIs, this was probably attributed to the different terminal functional groups of the polymers. Compared with the HBPIs derived from 1,3,5-tris[4-(4-amido-phenoxy)-phenyl]benzene (TAPOPB), a triamine monomer prepared by our previous work,[35] the T_g declines significantly. Free volume and strong electronegativity imparted by $-CF_3$ have high impact on the structure of FHBPIs.

The T_g data of the obtained FHBPIs were also investigated by DMTA. Figure 7b and c shows the curves of storage modulus and loss factor (tan δ). Obviously, the storage modulus decreases with the increasing temperature, whereas the loss factor increases first and then declines, and the temperature at the peak can be just considered as the T_g value of the FHBPI. Interestingly, these T_g values were slightly higher than those measured by DSC, which was mainly attributed to the difference in the detecting principle between the two measurements. Though the T_g values were different, the tendency was the same with dianhydride changes, (BTDA>6FDA>BPADA), as shown in Table 2. It is well-known that after macromolecules absorbed more energy to overcome the thermodynamic energy barrier, they would relax and move. Thus, the FHBPIs with the most rigid molecular chains (BTDA-based) relaxed at higher temperature.

In general, the temperature at 5% ($T_{d,5\%}$) and 10% ($T_{d,10\%}$) weight loss is usually used as a criterion factor to evaluate the thermal stability of polymers at high temperature. The thermal stabilities of the obtained FHBPIs were

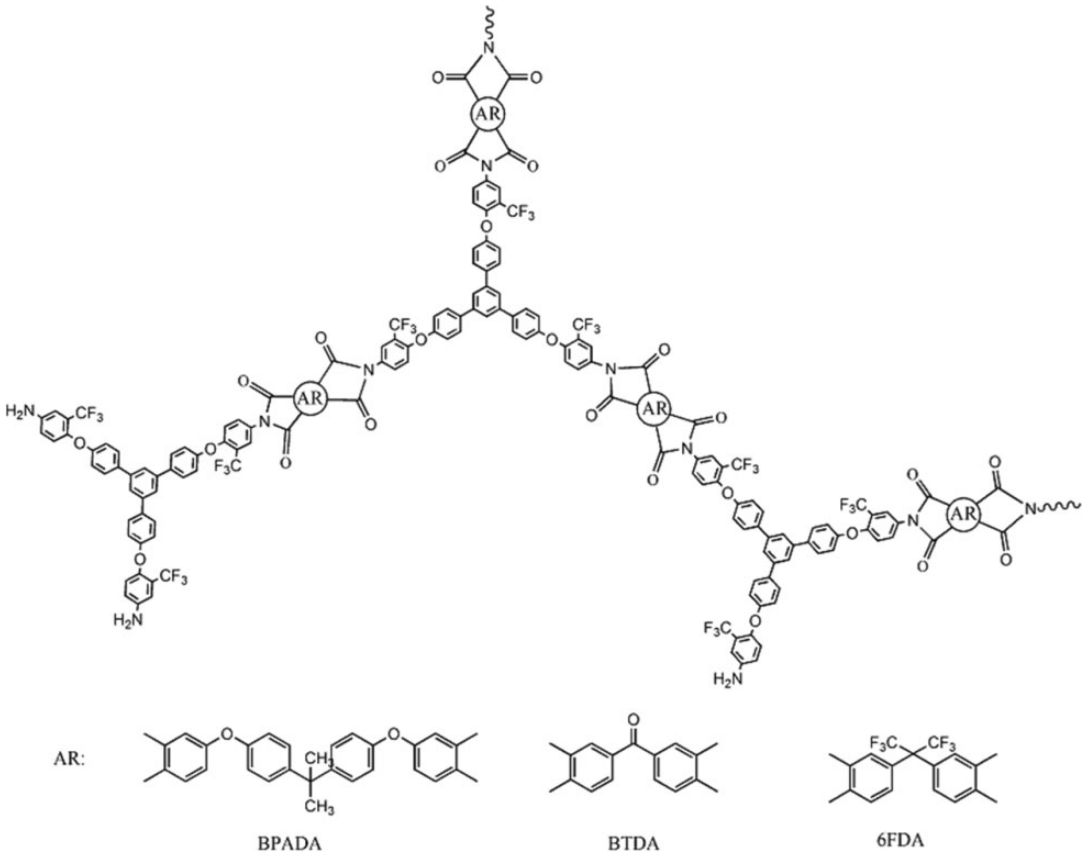

Figure 5. Partial chemical structure of the FHBPIs. FHBPIs: fluorinated hyperbranched polyimides.

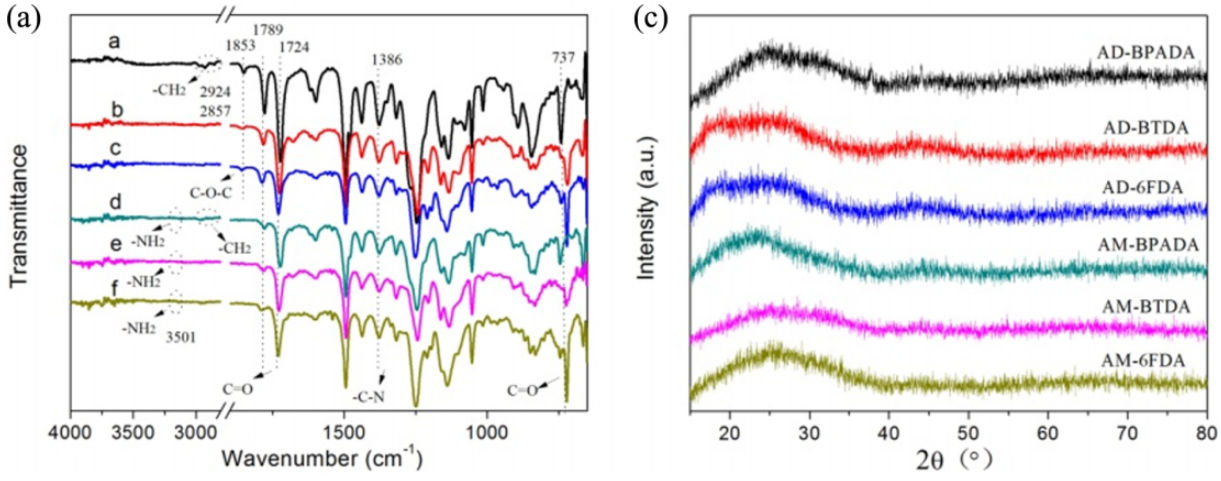

Figure 6. FTIR spectra curves (a) and XRD curves (b) of the resulting FHBPIs. FTIR: Fourier-transform infrared; XRD: X-ray powder diffraction; FHBPIs: fluorinated hyperbranched polyimides.

detected by TGA both in N_2 and in air atmosphere, as shown in Figure 8. Figure 8a and b shows the TGA curves of the resulting AM-FHBPIs and AD-HBPIs in nitrogen atmosphere. Because the PI molecule chains contain a large number of imide rings and benzene rings, all PIs exhibited excellent thermal stability. From the curves in Figure 8a, we can see that all FHBPIs had no obvious weight loss before 480°C in N_2 atmosphere. $T_{d,5\%}$ and $T_{d,10\%}$ were in the range of 482–518°C and 520–555°C, respectively, which can also be observed in Table 2. In addition, the percentage of residual weights ($R_{w\%}$) at 800°C was in the range of 56.2–63.6%. This also illustrated that the obtained FHBPIs

Table 1. Solubilities of the prepared FHBPIs.

Solvents									
Sample	NMP	DMF	DMAC	DMSO	Py	m-Cresol	THF	CH_2Cl_2	$CHCl_3$
AM-BPADA	++	++	++	++	++	++	++	+(++)	++
AM-BTDA	++	+(++)	++	+(++)	+(+)	+(++)	+(+)	-	+(+)
AM-6FDA	++	++	++	++	+(++)	+(++)	++	+(+)	+(++)
AD-BPADA	++	++	++	++	++	++	++	+(++)	++
AD-BTDA	++	+(++)	++	+(++)	+(+)	+(++)	+(+)	-	+(+)
AD-6FDA	++	++	++	++	+(++)	+(++)	++	+(+)	+(++)

NMP: *N*-methyl-2pyrrolidone; DMF: *N*, *N*-dimethyformamide; DMAC: *N*, *N*-dimethylacetamide; DMSO: dimethyl sulfoxide; Py: pyridine; THF: tetrahydrofuran; AM-BPADA: amino-terminated 2,2′-bis[4-(3,4-dicarboxyphenoxy)phenyl]propane dianhydride; AM-BTDA: amino-terminated 3′,4,4′-benzophenonetetracarboxylic dianhydride; AM-6FDA: amino-terminated 4,4-(hexafluoroisopropylidene) diphthalic anhydride; AD-BPADA: anhydride-terminated 2,2′-bis[4-(3,4-dicarboxyphenoxy)phenyl]propane dianhydride; AD-BTDA: anhydride-terminated 3′,4,4′-benzophenonetetracarboxylic dianhydride; AD-6FDA: 4,4-(hexafluoroisopropylidene) diphthalic anhydride; ++: soluble at room temperature; + soluble partially at room temperature; (): on heating, -: insoluble; FHBPIs: fluorinated hyperbranched polyimides.

Table 2. Thermal properties of the FHBPIs.

Polymer	T_g[a] (°C)	T_g[b] (°C)	$T_{d,5\%}$ (°C/N_2)	$T_{d,10\%}$ (°C/N_2)	$T_{d,5\%}$ (°C/air)	$T_{d,10\%}$ (°C/air)	R_w (%/N_2)	T_g[c] (°C)	$T_{d,5\%}$[d] (°C/N_2)	$T_{d,10\%}$[e] (°C/N_2)
AM-BPADA	235	258	513	545	490	527	63.6	270	444	502
AM-BTDA	264	337	516	553	509	530	60.6	316	479	560
AM-6FDA	257	326	510	540	495	530	58.3	–[f]	–	–
AD-BPADA	226	235	482	520	476	510	61.0	218	463	502
AD-BTDA	238	264	518	555	506	542	61.1	291	489	562
AD-6FDA	234	263	511	545	501	535	56.0	–	–	–

FHBPIs: fluorinated hyperbranched polyimides; DSC: differential scanning calorimetry; AM-BPADA: amino-terminated 2,2′-bis[4-(3,4-dicarboxyphenoxy) phenyl]propane dianhydride; AM-BTDA: amino-terminated 3′,4,4′-benzophenonetetracarboxylic dianhydride; AM-6FDA: amino-terminated 4,4-(hexafluoroisopropylidene) diphthalic anhydride; AD-BPADA: anhydride-terminated 2,2′-bis[4-(3,4-dicarboxyphenoxy)phenyl]propane dianhydride; AD-BTDA: anhydride-terminated 3′,4,4′-benzophenonetetracarboxylic dianhydride; AD-6FDA: 4,4-(hexafluoroisopropylidene) diphthalic anhydride.
[a]Glass transition temperatures by DSC.
[b]Glass transition temperature by DMA.
[c–e]The T_g and T_d data cited from our previous work by Li.[35]
[f]6FDA-based HBPI was not synthesized in our previous work by Li.[35]

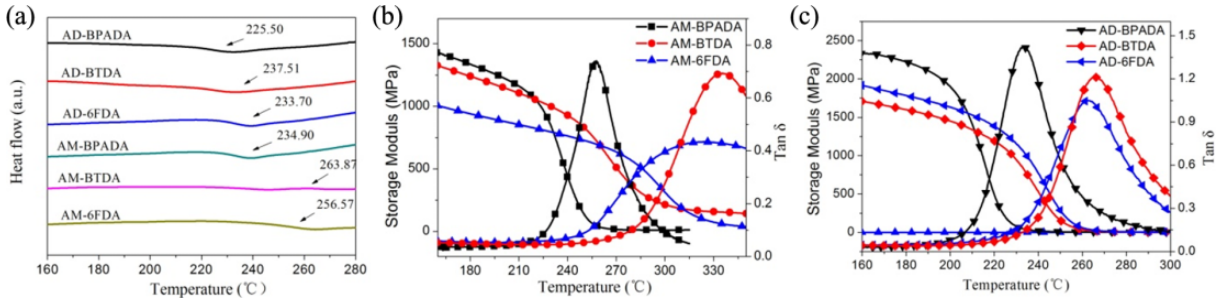

Figure 7. The DSC curves (a) and DMTA curves: (b) AD-FHBPIs, (c) AM-FHBPIs of FHBPIs. DSC: differential scanning calorimetry; DMTA: dynamical mechanical thermal analysis; AD-FHBPI: anhydride-terminated FHBPIs; AM-FHBPIs: amino-terminated FHBPIs; FHBPIs: fluorinated hyperbranched polyimides.

possessed good thermal stability in N_2. Figure 8c and d shows the TGA curves of the obtained FHBPIs in air. Compared with Figure 8a and b, the corresponding temperature values were slightly lower, and $R_{w\%}$ dropped sharply to zero in the range of 650–800°C. However, the trends in air and nitrogen are similar. $T_{d,5\%}$ and $T_{d,10\%}$ were in the range of 490–509°C and 527–541°C. Therefore, the FHBPIs also exhibited excellent thermo-oxidative stability in air. Furthermore, compared with the HBPIs derived from TAPOPB, a triamine monomer prepared by Li,[35] the $T_{d,5\%}$ and $T_{d,10\%}$ of the FHBPIs that we synthesized showed great improvement. This is mainly attributed to the excellent thermal stability

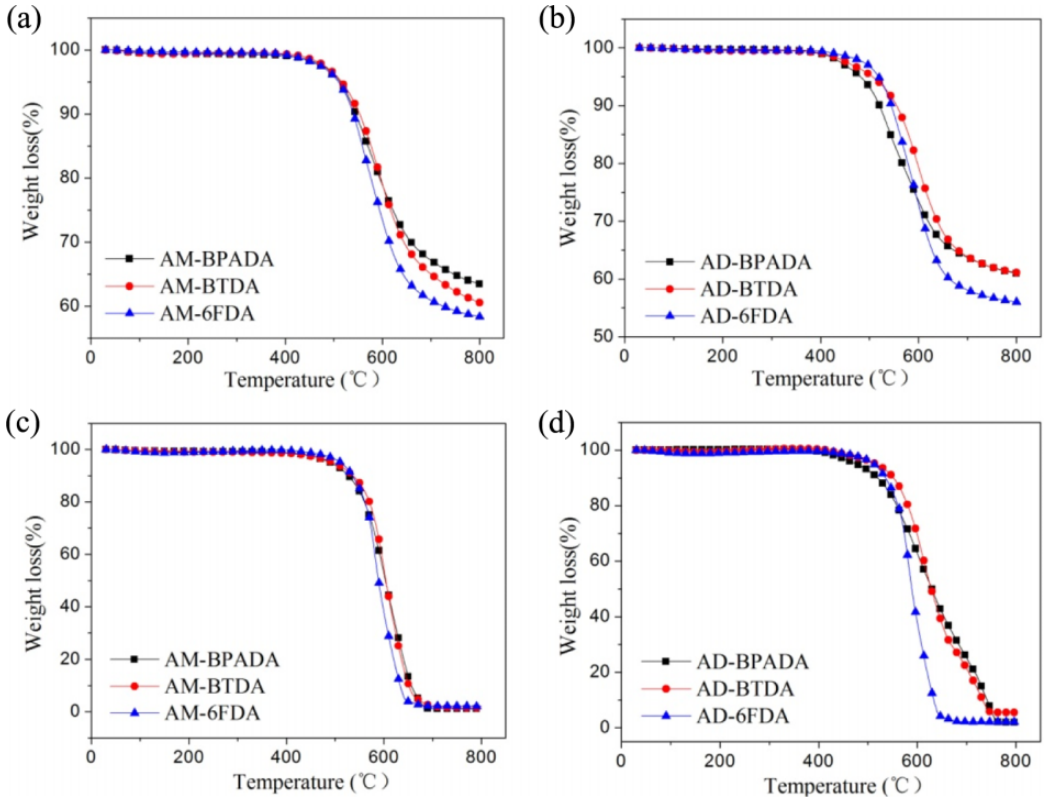

Figure 8. TGA curves of the FHBPIs in nitrogen atmosphere: (a) AM-FHBPIs, (b) AD-FHBPIs; TGA curves of the FHBPIs in air: (c) AM-FHBPIs, (d) AD-FHBPIs. TGA: thermogravimetric analysis; FHBPIs: fluorinated hyperbranched polyimides; AM-FHBPIs: amino-terminated FHBPIs; AD-FHBPI: anhydride-terminated FHBPIs.

and bulk volume of the $-CF_3$ from TTFPOPB. The bulk volume increases the free volume between the molecular chains, resulting in slow rate of heat transfer.

Mechanical properties of FHBPIs

The detailed data of mechanical properties for all films are listed in Table 3. The FHBPI films exhibited the average tensile strength in the range of 64.2–84.2 MPa, tensile modulus in the range of 1.2–1.5 GPa, and the elongation at the break between 6% and 10%. Additionally, the FHBPIs derived from BPADA got the biggest elongation at break and the least tensile strength and tensile modulus. This is due to the effects of the flexible segments from BPADA. Due to the rigid segments from BTDA, the AM-BTDA and AD-BTDA showed the smallest elongation at break but the highest tensile strength and tensile modulus. To sum up, the FHBPI films were strong and flexible materials.

Table 3. Mechanical properties of the resulting FHBPI films.

Polymer	Tensile strength (MPa)	Tensile modulus (GPa)	Elongation at break (%)
AM-BPADA	66.2	1.2	10
AM-BTDA	84.2	1.5	7
AM-6FDA	74.4	1.4	8
AD-BPADA	64.2	1.2	9
AD-BTDA	81.8	1.5	6
AD-6FDA	68.5	1.3	7

FHBPI: fluorinated hyperbranched polyimide; AM-BPADA: amino-terminated 2,2′-bis[4-(3,4-dicarboxyphenoxy)phenyl]propane dianhydride; AM-BTDA: amino-terminated 3′,4,4′-benzophenonetetracarboxylic dianhydride; AM-6FDA: amino-terminated 4,4-(hexafluoroisopropylidene) diphthalic anhydride; AD-BPADA: anhydride-terminated 2,2′-bis[4-(3,4-dicarboxyphenoxy)phenyl]propane dianhydride; AD-BTDA: anhydride-terminated 3′,4,4′-benzophenonetetracarboxylic dianhydride; AD-6FDA: 4,4-(hexafluoroisopropylidene) diphthalic anhydride.

Optical properties of FHBPIs

The fluorinated polymers are one of the most important high-performing polymers. Ascribed to the effects of the strong C–F bonds and strong electron withdrawing of the fluorine element in the chain structure, the fluorinated polymers are potential candidates for optical microelectronics and related industries. Figure 9 shows the UV-vis transmittance spectra of the obtained FHBPI films (ca. 0.16 mm). As shown in Table 4, we can see that the FHBPIs derived from 6FDA exhibited the highest optical transmittance, reaching about 93.5% and 94.5% of transmittance at

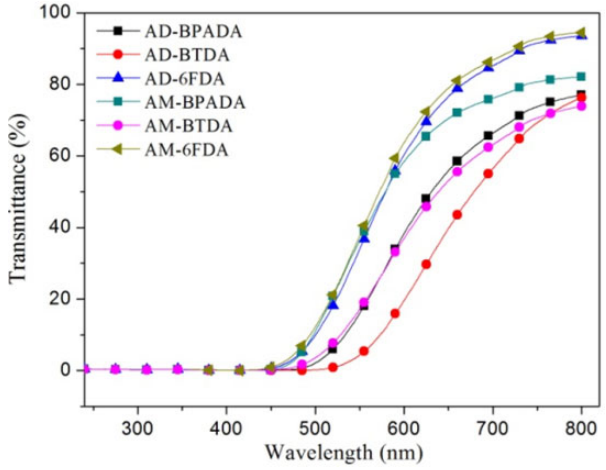

Figure 9. UV-vis transmittance spectra of the obtained FHBPIs. UV: ultraviolet; vis, visible; FHBPIs: fluorinated hyperbranched polyimides.

Table 4. Optical properties, SCA, and WA values of the resulting FHBPI films.

Sample	λ_0 (nm)	Transmittance at 800 nm (%)
AM-BPADA	441	82.1
AM-BTDA	444	73.9
AM-6FDA	431	94.5
AD-BPADA	456	77.0
AD-BTDA	495	76.3
AD-6FDA	425	93.5

SCA: surface contact angle; WA: water absorption; FHBPI: fluorinated hyperbranched polyimide; AM-BPADA: amino-terminated 2,2′-bis[4-(3,4-dicarboxyphenoxy)phenyl]propane dianhydride; AM-BTDA: amino-terminated 3′,4,4′-benzophenonetetracarboxylic dianhydride; AM-6FDA: amino-terminated 4,4-(hexafluoroisopropylidene) diphthalic anhydride; AD-BPADA: anhydride-terminated 2,2′-bis[4-(3,4-dicarboxyphenoxy)phenyl]propane dianhydride; AD-BTDA: anhydride-terminated 3′,4,4′-benzophenonetetracarboxylic dianhydride; AD-6FDA: 4,4-(hexafluoroisopropylidene) diphthalic anhydride.

800 nm, and the truncation wavelength is 425 and 431 nm, respectively. The transmittance of FHBPIs derived from BTDA and BPADA is around 80% at 800 nm. It is indicated that the transmittance of the FHBPIs is increased with the increasing fluorine content. The truncation wavelengths of all the FHBPIs were greater than 420 nm, and to our knowledge, the wavelength of UV was in the range of 10–400 nm, which was below the truncation wavelength of the FHBPIs. Compared with the HBPIs derived from TAPOPB, a triamine monomer prepared by Li,[35] the transmittance at visible area and truncation wavelength of the FHBPIs that we synthesized showed much improvement, which is also attributed to the bulk volume and high polarity of the $-CF_3$ from TTFPOPB. Therefore, the prepared FHBPIs could be promising UV-shielding materials.

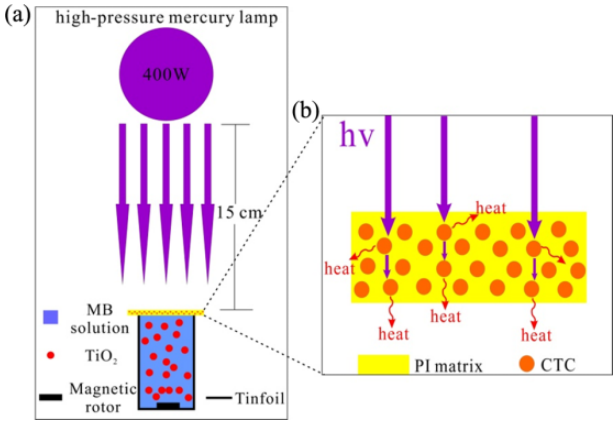

Figure 10. Simulation illustration for UV-shielding measurement (a); Schematic diagram for UV-shielding of FHBPI films (b). UV: ultraviolet; FHBPI: fluorinated hyperbranched polyimide.

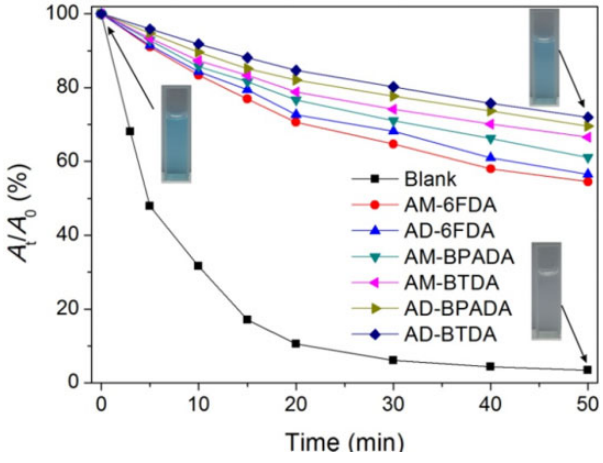

Figure 11. Decay curves of the absorption intensity of the MB solution at 665 nm under no protection and protected by FHBPI films. MB: methylene blue; FHBPI: fluorinated hyperbranched polyimide.

UV-shielding performance of FHBPIs

To further examine the UV-shielding performance, photocatalytic degradation of MB solution in the presence of TiO_2 nanoparticles was carried out, as shown in Figure 10a. Figure 10b exhibits the schematic diagram for UV shielding of the FHBPI films. Because a number of CTCs that exist in the molecule or between molecules of FHBPI and CTC can absorb UV, FHBPI films are endowed with the function of UV absorption. To quantify the shielding efficiency of all films, the decay curves of the absorption intensity of the MB solution at 665 nm are shown in Figure 11. As a blank control experiment, the intensity of the absorption at 665 nm gradually decreases with time. The absence of the films for shielding the MB solution results in a complete degradation after irradiation for 50 min. This indicates that the efficiency of reducing MB is very high when directly exposed to the intense UV light

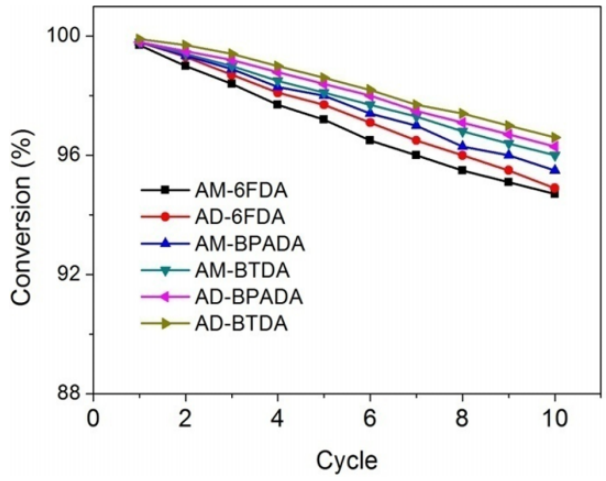

Figure 12. Recyclability of FHBPI films as a UV-shielding materials for MB solution. FHBPI: fluorinated hyperbranched polyimide; UV: ultraviolet; MB: methylene blue.

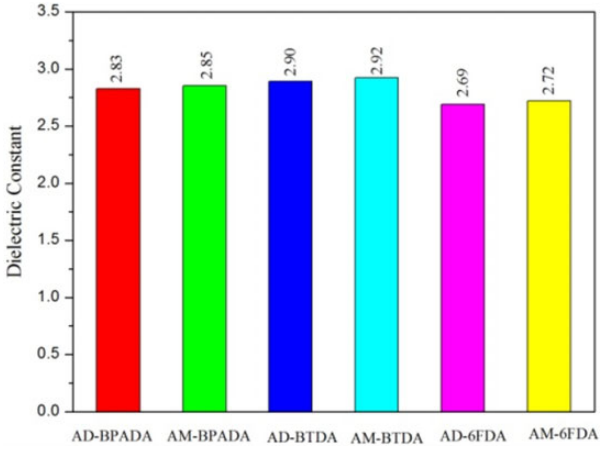

Figure 13. Dielectric constant of the resulting FHBPIs. FHBPIs: fluorinated hyperbranched polyimides.

(400 W) in the presence of TiO_2 nanoparticles. After being protected by FHBPI films, the degradation rate of MB solution obviously decreased. MB solution protected with AM-6FDA displayed the maximum degradation among them, which reached 54% after UV irradiation for 50 min. The minimal degradation was obtained from MB solution protected with AD-BTDA, reaching 27% after UV irradiation for 50 min. It can be seen from Figure 11 that the shielding efficiency is as follows: BTDA-based FHBPI > BPADA-based FHBPI > 6FDA-based FHBPI. This is mainly related to the number of CTCs. The molecular chains of 6FDA-based FHBPI are not arranged closely due to $-CF_3$, which results in a significant reduction in CTC between molecules. BTDA-based FHBPIs possess more electronic donors (aromatic amine monomeric unit) and electron acceptors (aromatic dianhydride monomeric unit), which are closer than those in BPADA-based FHBPI. Thus, more CTCs are formed in BTDA-based FHBPI. Compared with the original MB solution, the solution in blank control experiment showed an obvious discoloration due to the large photodegradation of MB solution, whereas the solution protected with AD-BTDA film displayed a slight change after UV irradiation and was similar to the original color of the MB solution. Additionally, the films exhibited high optical transmittance at 800 nm in visible area. The above results revealed that FHBPI films had excellent UV-shielding performance and may be used as UV-shielding material in the environment filled with high temperature and intensive UV light.

Another important factor of the UV-shielding materials, besides the UV-shielding efficiency, is the recyclability of the UV-shielding materials for the assessment of the resistance to UV exposure. To study the recyclability of these FHBPI films, repeated experiments for UV shielding of MB solution were performed. These FHBPI films show similar UV-shielding activities, only slight decrease, and the conversion is still greater than 94% after running 10 cycles (Figure 12). Hence, the prepared FHBPI films have been proven to be potential recyclable UV-shielding materials.

Table 5. Weight-average M_w, PDI, surface contact angle, and water absorption.

Sample	M_w[a]	PDI	SCA (°)	WA (%)
AM-BPADA	85,000	1.31	102.0	0.50
AM-BTDA	–[b]	–	100.0	0.68
AM-6FDA	76,000	1.34	98	0.70
AD-BPADA	30,000	1.65	99.0	0.72
AD-BTDA	–	–	100.5	0.61
AD-6FDA	24,000	1.71	100.0	0.62

M_w: molecular weight; PDI: polydispersity index; GPC: gel permeation chromatography; THF: tetrahydrofuran; SCA: surface contact angle; WA: water absorption; AM-BPADA: amino-terminated 2,2′-bis[4-(3,4-dicarboxyphenoxy)phenyl]propane dianhydride; AM-BTDA: amino-terminated 3′,4,4′-benzophenonetetracarboxylic dianhydride; AM-6FDA: amino-terminated 4,4-(hexafluoroisopropylidene) diphthalic anhydride; AD-BPADA: anhydride-terminated 2,2′-bis[4-(3,4-dicarboxyphenoxy) phenyl]propane dianhydride; AD-BTDA: anhydride-terminated 3′,4,4′-benzophenonetetracarboxylic dianhydride; AD-6FDA: 4,4-(hexafluoroisopropylidene) diphthalic anhydride.
[a]The weight-average M_w and PDI were measured by GPC using THF solution.
[b]Not measured for insoluble or slightly soluble in THF.

Dielectric constant

The dielectric constants of the resulting FHBPIs were in the range of 2.69–2.92 at 1 MHz, as shown in Figure 13. It can be seen that the FHBPIs derived from 6FDA have the lowest dielectric constant (AD-6FDA, 2.69; AM-6FDA, 2.72). The dielectric constants of AD-BPADA and AM-BPADA were a little lower than the AD-BTDA and AM-BTDA, and the specific values are 2.83 for AD-BPADA, 2.85 for

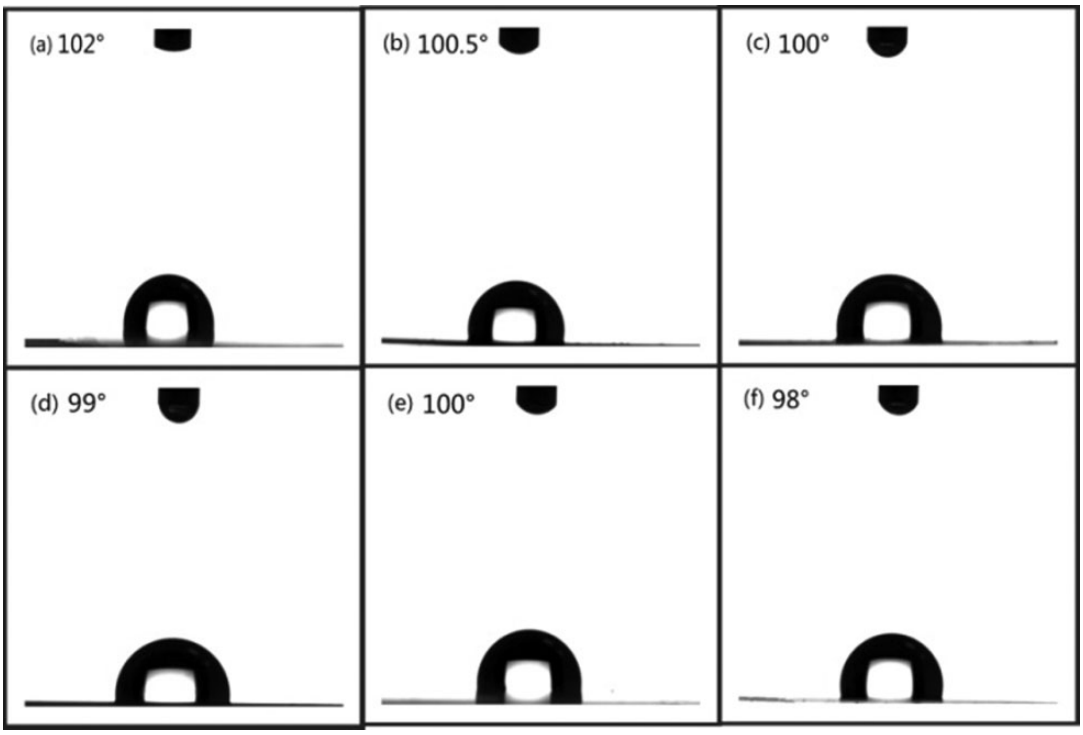

Figure 14. Surface contact angle of FHBPIs. (a) AD-BPADA, (b) AD-BTDA, (c) AD-6FDA, (d) AM-BPADA, (e) AM-BTDA, (f) AM-6FDA. FHBPIs: fluorinated hyperbranched polyimides; AD-BPADA: anhydride-terminated 2,2′-bis[4-(3,4-dicarboxyphenoxy)phenyl]propane dianhydride; AD-BTDA: anhydride-terminated 3′,4,4′-benzophenonetetracarboxylic dianhydride; AD-6FDA: 4,4-(hexafluoroisopropylidene) diphthalic anhydride; AM-BPADA: amino-terminated 2,2′-bis[4-(3,4-dicarboxyphenoxy)phenyl]propane dianhydride; AM-BTDA: amino-terminated 3′,4,4′-benzophenonetetracarboxylic dianhydride; AM-6FDA: amino-terminated 4,4-(hexafluoroisopropylidene) diphthalic anhydride.

AM-BPADA, 2.90 for AD-BTDA, and 2.92 for AM-BTDA. The differences are mainly attributed to the structure of the dianhydride monomers. 6FDA possesses the bulky $-CF_3$ groups, which resulted in less efficient chain packing and increased free volume. Moreover, the strong electronegativity of fluorine atoms would result in very low C–F polarizability; the ether bonds in BPADA could increase the flexibility of the polymer chains and dilution effect of the polar imide ring; and the ketonic linkages from BTDA will lead to a high dielectric constant. On the other hand, there are several $-CF_3$ groups, ether bonds, and prolonged segments in TTFPOPB, reducing the dielectric constants of the FHBPIs significantly, compared with the early reports.[37–39]

Weight-average M_w, water absorption (WA), and surface contact angle (SCA)

According to the data from Table 5, the weight-average M_ws of AM-BPADA and AM-6FDA were 85,000 and 76,000, respectively, which were obviously greater than that of AD-BPADA (30,000) and AD-6FDA (24,000). This was mainly attributed to the different imidization methods. The one-step method could provide sufficient energy to the polymerization reaction and give high-M_w PIs. The M_ws of BTDA-based PIs could not be measured for slight solubility in THF.

Figure 14 shows the surface contact angle of the FHBPIs. Due to the high content of fluorine element, all of the resulting FHBPI films showed average SCA around 100°; this demonstrated that the obtained FHBPIs were basically hydrophobic. Furthermore, the SCAs of the AD-FHPBPI films were slightly bigger than the AM-FHBPI films, which might be attributed to the hydrophobic of the terminal groups. In addition, WAs of the FHBPIs are small, which are 0.50–0.72%, as shown in Table 5. Therefore, the resulting FHBPIs might be promising hydrophobic materials.

Conclusion

A novel aromatic triamine, TTFAPOPB, with three symmetrical prolonged chain segments, ether bonds, and $-CF_3$ groups, was successfully synthesized. Then the synthesized TTFAPOPB and commercially available dianhydride (BPADA, BTDA, 6FDA) were further used as monomers to prepare a series of fluorine hyperbranched PIs (AD-FHBPIs and AM-FHBPIs). FT-IR, ^{1}H NMR, and element analysis showed that the obtained triamine monomer was

pure and stable. As expected, the obtained FHBPIs had a low degree of crystallinity, predominantly amorphous structure, and good solubility. Meanwhile, the FHBPIs also exhibited excellent thermal stability both in air and in N_2 atmosphere, good mechanical properties, considerable optical transparency, and brilliant UV-shielding performance. With good UV absorption and low water absorption, the FHBPIs might be promising materials in the field of UV-shielding materials in high-temperature environment. In addition, because of the high content of $-CF_3$ groups, the FHBPIs possess excellent hydrophobic properties and low dielectric constants. It might be useful in the field of electronic.

Acknowledgments

Meanwhile, authors also acknowledge the Ministry of Education Key Laboratory for the Green Preparation and Application of Functional Materials for providing necessary facilities.

Authors' contribution

Qing Li and Shulai Zhang contributed equally to this work.

Declaration of Conflicting Interests

The author(s) declared no potential conflict of interest with respect to the research, authorship, and/or publication of this article.

Funding

The author(s) disclosed receipt of the following financial support for the research, authorship, and/or publication of this article: the Natural Science Foundation of Hubei Province (2013CFB007), Hubei, China.

References

1. Cabanetos C, Blart E, Pellegrin Y, et al. Synthesis and second-order nonlinear optical properties of a crosslinkable functionalized hyperbranched polymer. *Eur Polym J* 2012; **48**(1): 116–126.
2. Caminade AM, Yan D and Smith DK. Dendrimers and hyperbranched polymers. *Chem Soc Rev* 2015; **44**(12): 3870–3873.
3. Morikawa A and Akagi M. Hyperbranched poly(ether ether ketone)s: preparation and comparison of properties with the corresponding dendrimers. *Polym J* 2013; **45**(6): 614–621.
4. Zheng Y, Li S, Weng Z, et al. Hyperbranched polymers: advances from synthesis to applications. *Chem Soc Rev* 2015; **44**(12): 4091–4130.
5. Cao Z, Lin J, Liu Y, et al. Crosslinkable fluorinated hyperbranched polyimide for thermo-optic switches with high thermal stability. *J Appl Polym Sci* 2012; **127**(1): 607–611.
6. Sohn GJ, Choi HJ, Jeon IY, et al. Water-dispersible, sulfonated hyperbranched poly(ether-ketone) grafted multiwalled carbon nanotubes as oxygen reduction catalysts. *Acs Nano* 2013; **6**(7): 6345–6355.
7. Zhang H, Patel A, Gaharwar AK, et al. Hyperbranched polyester hydrogels with controlled drug release and cell adhesion properties. *Biomacromolecules* 2013; **14**(5): 1299–1310.
8. Wu C, Huang X, Wang G, et al. Hyperbranched-polymer functionalization of graphene sheets for enhanced mechanical and dielectric properties of polyurethane composites. *J Mater Chem* 2012; **22**(14): 7010–7019.
9. Yadav SK, Mahapatra SS and Cho JW. Synthesis of mechanically robust antimicrobial nanocomposites by click coupling of hyperbranched polyurethane and carbon nanotubes. *Polymer* 2012; **53**(10): 2023–2031.
10. Wu W, Tang R, Li Q, et al. Functional hyperbranched polymers with advanced optical, electrical and magnetic properties. *Chem Soc Rev* 2015; **44**(12): 3997–4022.
11. Shaplov AS, Marcilla R and Mecerreyes D. Recent advances in innovative polymer electrolytes based on poly(ionic liquid)s. *Electrochim Acta* 2015; **175**: 18–34.
12. Dey P, Blakey I, Thurecht KJ, et al. Self-assembled hyperbranched polymer–gold nanoparticle hybrids: understanding the effect of polymer coverage on assembly size and SERS performance. *Langmuir* 2013; **29**(2): 525–533.
13. Jin H, Huang W, Zhu X, et al. Biocompatible or biodegradable hyperbranched polymers: from self-assembly to cytomimetic applications. *Chem Soc Rev* 2012; **41**(18): 5986–5997.
14. Lazo MAG, Teuscher R, Leterrier Y, et al. UV-nanoimprint lithography and large area roll-to-roll texturization with hyperbranched polymer nanocomposites for light-trapping applications. *Sol Energ Mat Sol C* 2012; **103**: 147–156.
15. Jiang Q, Wang X, Zhu Y, et al. Mechanical, electrical and thermal properties of aligned carbon nanotube/polyimide composites. *Compos B Eng* 2014; **56**: 408–412.
16. Koerner H, Strong RJ, Smith ML, et al. Polymer design for high temperature shape memory: Low crosslink density polyimides. *Polymer* 2013; **54**(1): 391–402.
17. Liu Y, Yu C, Jin H, et al. A supramolecular Janus hyperbranched polymer and its photoresponsive self-assembly of vesicles with narrow size distribution. *J Am Chem Soc* 2013; **135**(12): 4765–4770.
18. Meador MAB, McMillon E, Sandberg A, et al. Dielectric and other properties of polyimide aerogels containing fluorinated blocks. *Acs Appl Mater Inter* 2014; **6**(9): 6062–6068.
19. Ni HJ, Liu JG, Wang ZH, et al. A review on colorless and optically transparent polyimide films: Chemistry, process and engineering applications. *J Ind Eng Chem* 2015; **28**: 16–27.
20. Buonocore GG, Schiavo L, Attianese I, et al. Hyperbranched polymers as modifiers of epoxy adhesives. *Compos B Eng* 2013; **53**(7): 187–192.
21. Kim S, Wang X, Ando S, et al. Low dielectric and thermally stable hybrid ternary composites of hyperbranched and linear polyimides with SiO_2. *Rsc Adv* 2014; **4**(52): 27267–27276.
22. Lei XF, Chen Y, Zhang HP, et al. Space survivable polyimides with excellent optical transparency and self-healing properties derived from hyperbranched polysiloxane. *Acs Appl Mater Int* 2013; **5**(20): 10207–10220.

23. Liu JC, Lin L, Jia X, et al. Synthesis and properties of UV-curable hyperbranched polyurethane and its application in the negative-type photoresist. *J Wuhan Univ Technol* 2014; **29**(1): 208–212.
24. Rogan Y, Malpassevans R, Carta M, et al. A highly permeable polyimide with enhanced selectivity for membrane gas separations. *J Mater Chem A* 2014; **2**(14): 4874–4877.
25. Zhang Y, Shen J, Li Q, et al. Synthesis and characterization of novel hyperbranched polyimides/attapulgite nanocomposites. *Compos A Appl S* 2013; **55**(6): 161–168.
26. Yi L, Li C, Huang W, et al. Soluble and transparent polyimides with high Tg from a new diamine containing tert-butyl and fluorene units. *J Polym Sci Pol Chem* 2016; **54**(7): 976–984.
27. Li Q, Wang Y, Zhang SL, et al, Novel fluorinated random copolyimide/amine-functionalized zeolite MEL50 hybrid films with enhanced thermal and low dielectric properties, *J Mater Sci* 2017; **52**: 5283–5296.
28. Li Q, Liao GF, Zhang SL, et al. Effect of adjustable molecular chain structure and pure silica zeolite nanoparticles on thermal, mechanical, dielectric, UV-shielding and hydrophobic properties of fluorinated copolyimide composites. *Appl Surf Sci* 2018; **427**: 437–450.
29. Dhara MG and Banerjee S. Fluorinated high-performance polymers: poly(arylene ether)s and aromatic polyimides containing trifluoromethyl groups. *Prog Polym Sci* 2010; **35**(8): 1022–1077.
30. Liu C, Pei X, Huang X, et al. Novel non-coplanar and tertbutyl-substituted polyimides: solubility, optical, thermal and dielectric properties. *Chinese J Chem* 2015; **33**(2): 277–284.
31. Kalita H and Karak N. Hyperbranched polyurethane/Fe_3O_4 thermosetting nanocomposites as shape memory materials. *Polym Bull* 2013; **70**(11): 2953–2965.
32. Lei X, Chen Y, Qiao M, et al. Hyperbranched polysiloxane (HBPSi)-based polyimide films with ultralow dielectric permittivity, desirable mechanical and thermal properties. *J Mater Chem C* 2016; **4**(11): 2134–2146.
33. Fang J, Hidetoshi Kita A and Okamoto K. Hyperbranched polyimides for gas separation applications. 1. synthesis and characterization. *Macromolecules* 2000; **33**(13): 4639–4646.
34. Hong G, Dong W, Guan S, et al. Fluorinated hyperbranched polyimide for optical waveguides. *Macromol Rapid Comm* 2010; **28**(3): 252–259.
35. Li Q, Xiong H, Pang L, et al. Synthesis and characterization of thermally stable, hydrophobic hyperbranched polyimides derived from a novel triamine. *High Perform Polym* 2015; **27**(4): 426–438.
36. Shen J, Zhang Y, Chen W, et al. Synthesis and properties of hyperbranched polyimides derived from novel triamine with prolonged chain segments. *J Polym Sci Pol Chem* 2013; **51**(11): 2425–2437.
37. Chen W, Li Q, Zhang Q, et al. Fabrication and characterization of novel hyperbranched polyimides with excellent organosolubility, thermal and mechanical properties. *J Appl Polym Sci* 2015; **132**(9): 237–244.
38. Wooley KL, Hawker CJ, Lee R, et al. One-step synthesis of hyperbranched polyesters. Molecular weight control and chain end functionalization. *Polym J* 1994; **26**(2): 187–197.
39. Hsiaoa SH, Chung CL and Chen WT. Synthesis and characterization of novel fluorinated polyimides derived from 1,3-bis(4-amino-2-trifluoromethylphenoxy)naphthalene and aromatic dianhydrides. *Eur Polym J* 2010; **46**(9): 1878–1890.